
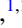








Relationship between the hydroxyl termination and band bending at ($\bar{2}01$) β -Ga₂O₃ surfaces

R. M. Gazoni ^{1,2}, L. Carroll ^{1,2}, J. I. Scott ^{1,2}, S. Astley ³, D. A. Evans ³, A. J. Downard ^{1,2},
R. J. Reeves ^{1,2} and M. W. Allen ^{2,4}

¹*School of Physical and Chemical Sciences, University of Canterbury, Christchurch 8041, New Zealand*

²*MacDiarmid Institute for Advanced Materials and Nanotechnology, Wellington 6140, New Zealand*

³*Department of Physics, Aberystwyth University, Aberystwyth, Ceredigion, SY23 3BZ United Kingdom*

⁴*Department of Electrical and Computer Engineering, University of Canterbury, Christchurch 8041, New Zealand*



(Received 16 April 2020; revised 7 June 2020; accepted 9 June 2020; published 13 July 2020)

Synchrotron x-ray photoelectron spectroscopy was used to explore the relationship between the hydroxyl termination and band bending at the ($\bar{2}01$) surface of β -Ga₂O₃ bulk single crystals. All as-received ($\bar{2}01$) surfaces were terminated with OH groups, with H/OH binding to surface O_s/Ga_s atoms. Removal of this native OH termination produced a large upward shift in band bending of up to 1.0 eV, consistent with strong electron depletion and a semiconductor to insulator-like transition in the near-surface region. Simple surface treatments were used to control the size and stability of the band bending of as-received ($\bar{2}01$) surfaces by modifying the nature of the OH termination. NaOH (H₂SO₄) treatment consistently produced upward (downward) shifts in band bending and a significant increase (decrease) in the thermal stability of the OH termination that was associated with an increase in the relative density of Ga_s-OH (O_s-H) species. Annealing in wet O₂ (at 600 °C) produced an extremely stable OH termination and the strongest downward shift in band bending. These effects, combined with the relatively slow dissociation of H₂O on bare ($\bar{2}01$) surfaces, allowed the preparation of surfaces with significant variations in band bending that may prove useful in optimizing the properties of β -Ga₂O₃ metal-semiconductor contacts and heterojunctions. A comparison of two methods used to determine the absolute band bending at semiconductor surfaces confirmed that bare β -Ga₂O₃ ($\bar{2}01$) surfaces are characterized by strong upward band bending (~ 0.5 to 1.0 eV) and an electron depletion layer that can be completely removed by the hydroxylation of the surface.

DOI: [10.1103/PhysRevB.102.035304](https://doi.org/10.1103/PhysRevB.102.035304)

I. INTRODUCTION

Monoclinic β -Ga₂O₃ is an ultrawide-band-gap semiconductor that has become the subject of considerable interest for power electronic devices and deep UV photodetectors [1–3]. It has one of the highest known breakdown fields (~ 8 MV/cm), significantly higher than that of SiC or GaN (~ 3 MV/cm), allowing the potential scaling of next-generation power Schottky diodes and field-effect transistors to smaller dimensions, thereby increasing their speed and efficiency. However, device fabrication is still at an early stage and a thorough understanding of the electronic nature of the commonly used surfaces of β -Ga₂O₃ is required to optimize the performance of metal-semiconductor contacts and heterojunctions with other semiconductors [4,5].

The surfaces of β -Ga₂O₃ are also interesting from a fundamental perspective as they appear to show significant differences in electronic behavior compared to other technologically useful transparent conducting oxides (TCOs), such as ZnO [6], SnO₂ [7], CdO [8], and In₂O₃ [9,10]. The surfaces of the latter TCOs have a metalliclike nature due to the presence of a two-dimensional electron accumulation layer that is confined inside a potential well created by the downward bending of the near-surface electronic bands in response to donorlike surface states [6–12]. In the case of ZnO, we have previously reported a strong correlation between the downward band bending and the OH termination

of the surface, with a reduction in OH coverage producing a transition from surface electron accumulation to depletion [13,14]. The surface metallicity of ZnO, SnO₂, and In₂O₃ also results in a number of interesting physical effects: (i) a difficulty in forming high-quality Schottky metal-semiconductor contacts without the use of oxidizing surface treatments, such as an oxygen plasma, ozone, or hydrogen peroxide, to reduce the surface conductivity [15–18], and (ii) the tendency of the electron-rich surfaces to attract electrophilic atmospheric adsorbates, such as O₂ and H₂O, and introduce environmental sensitivity into the performance of electronic devices [19–21].

In contrast, β -Ga₂O₃ surfaces appear to be naturally depleted of charge carriers and several researchers have used x-ray photoelectron spectroscopy (XPS) to report significant upward band bending at β -Ga₂O₃ surfaces: Navarro-Quezada *et al.* [22] used Al K α ($h\nu = 1486.6$ eV) XPS to measure an upward band bending of ~ 0.28 eV at air-cleaved β -Ga₂O₃ (100) surfaces that increased to ~ 0.48 eV after annealing at 800 °C, while Lovejoy *et al.* [23] used hard XPS and scanning tunneling microscopy on nominally undoped β -Ga₂O₃ (100) surfaces to observe an upward band bending of ~ 0.5 eV and the presence of negatively charged surface defects. Both these results appear consistent with experimental observations that (i) Ohmic contacts are rather difficult to produce on β -Ga₂O₃, typically requiring postmetallization annealing [24,25], while the formation of high-quality Schottky contacts is relatively straightforward [26,27], i.e., the opposite situation

to that observed in ZnO, SnO₂, and In₂O₃ [15–18], and (ii) simple electrical measurements using standard metal probes yield very high resistances even on low-resistivity Sn-doped β -Ga₂O₃ substrates, suggesting the presence of an electrically inactive surface layer [23].

However, the assumption that β -Ga₂O₃ surfaces are naturally depleted of charge carriers has recently been questioned by the work of Swallow *et al.* [28], who proposed that the upward band bending at β -Ga₂O₃ surfaces determined by XPS measurements has been significantly overestimated, by as much as ~ 0.5 eV. The standard XPS method of determining the band bending at semiconductor surfaces is to use the intersection of a linear extrapolation of the low binding energy (BE) edge of the valence-band spectrum with the instrument background to determine the band-bending parameter ζ [29]. This is the energetic separation between the valence-band maximum (E_V) and the Fermi level (E_F) at a depth approximately equal to the inelastic mean-free path (λ) of the XPS photoelectrons. The actual band bending (V_{bb}) is then determined from

$$V_{bb} = E_g - \zeta - \xi, \quad \text{where } \xi = kT/q \ln(N_C/n), \quad (1)$$

E_g is the band gap of the semiconductor, and $\xi (= E_C - E_F)$ is the energy separation between the conduction-band minimum (E_C) and E_F , with n the bulk carrier concentration and N_C the conduction-band effective density of states [$N_C = 2(2\pi m_e^* kT/h^2)^{3/2}$]. For β -Ga₂O₃, $N_C = 3.72 \times 10^{18} \text{ cm}^{-3}$ at $T = 300 \text{ K}$, assuming an effective electron mass m_e^* of $0.28m_e$ [30,31]. Negative values of V_{bb} indicate downward surface band bending and electron accumulation, while positive values of V_{bb} correspond to upward band bending and electron depletion.

Swallow *et al.* [28] argued that in the case of β -Ga₂O₃ (and also In₂O₃) instrumental broadening of the XPS measured valence-band (VB) edge causes an underestimation of ζ due to the very rapid onset of the valence-band density of states (VB-DOS) that results from the very low dispersion at the valence-band maximum. Instead, they proposed a method of fitting an instrumental and lifetime-broadened VBDOS calculated using hybrid density-functional theory to their experimental VB XPS spectra, with the almost-vertical leading edge of the corresponding unbroadened VBDOS used to determine ζ . This VBDOS-fitting method resulted in a systematic increase in ζ of ~ 0.5 eV, sufficient for these authors to report a downward band bending of ~ 0.24 eV and therefore electron accumulation at the as-received (“uncleaned”) surfaces of their β -Ga₂O₃ ($\bar{2}01$) single-crystal substrates, instead of an upward band bending of approximately the same amount that would have been determined using the standard linear VB-edge extrapolation method [29].

There is evidence to suggest that hydrogen in the form of hydroxyl (OH) groups acts as a surface donor in β -Ga₂O₃ producing a downward shift in band bending at the surface. Swallow *et al.* [28] observed that the *in situ* cleaning of the ($\bar{2}01$) surface by thermal annealing up to 800°C produced an upward shift in band bending of ~ 0.5 eV that was correlated with the removal of OH from the surface. A similar upward shift was reported by Navarro-Quezada *et al.* [22] on (100) β -Ga₂O₃ single crystals after *in situ* annealing to the same

temperature. Both these studies used Al $K\alpha$ ($h\nu = 1486.6 \text{ eV}$) XPS with a relatively deep sampling depth ($\lambda \sim 18 \text{ \AA}$) and the band-bending changes closer to the surface are likely to be significantly larger. In the case of ZnO ($10\bar{1}0$) and ($000\bar{1}$) surfaces, we have previously used synchrotron XPS ($h\nu = 150 \text{ eV}$, $\lambda \sim 6.8 \text{ \AA}$) to observe upward band-bending shifts of ~ 0.8 eV after significantly reducing the surface OH termination, sufficient to produce strong near-surface electron depletion [13,14].

In this work, we use surface-sensitive synchrotron XPS to determine the relationship between the OH termination and the electronic band bending at the ($\bar{2}01$) surface of β -Ga₂O₃. This is one of the most common low-index surfaces involved in bulk single crystal and epitaxial thin-film growth. Due to the large number of atoms and low symmetry of the unit cell, there are several possible structures for the ($\bar{2}01$) surface depending on the cleavage plane chosen [see Fig. 1(a)]. Density-functional theory (DFT) calculations by Anvari *et al.* [32] have indicated that the most likely of these are two nonpolar stoichiometric ($\bar{2}01$) surfaces. Here, we will consider one of these surfaces as shown in Fig. 1(b). This is the relaxed surface created after cutting the fewest number of Ga_I-O_{II} bonds. However, our analysis also applies to the alternative structure considered by Anvari *et al.* [32], given that both have the same surface density of Ga and O atoms and that there is only a small (9 meV \AA^{-2}) difference in their surface energy. We show that bare ($\bar{2}01$) β -Ga₂O₃ surfaces are characterized by strong upward band bending (~ 0.5 to 1.0 eV) and an electron depletion layer that can be completely removed by the hydroxylation of the surface. We also show that different surface treatments can be used to modify the nature and stability of the OH termination and allow ($\bar{2}01$) β -Ga₂O₃ surfaces with significant variations in surface band bending (up to ~ 1 eV) to be prepared. The ability to control the band bending of β -Ga₂O₃ surfaces may prove useful in optimizing the fabrication of metal-semiconductor contacts and semiconductor-semiconductor heterojunctions to this technologically useful material.

II. EXPERIMENTAL METHODS

A. Surface treatments

The β -Ga₂O₃ material used in this study was a Sn-doped ($\bar{2}01$) single-crystal wafer of dimensions $15 \times 10 \times 0.65 \text{ mm}^3$, from Tamura Corporation (Japan). This was grown using the edge-defined film-fed growth method [33], with a resistivity, carrier density, and mobility of $0.020 \text{ } \Omega \text{ cm}$, $4.46 \times 10^{18} \text{ cm}^{-3}$, and $71 \text{ cm}^2 \text{ V}^{-1} \text{ s}^{-1}$, respectively, as determined by 0.51-T Hall effect measurements at room temperature (RT). The band gap of the ($\bar{2}01$) β -Ga₂O₃ wafer was $4.71 \pm 0.02 \text{ eV}$, as determined from optical transmission spectroscopy, also at RT (see Supplemental Material Fig. S1 [34]). The wafer was evenly diced to provide ($5 \times 5 \times 0.65 \text{ mm}^3$) samples that were cleaned using ultrasonically agitated acetone, methanol, and isopropyl alcohol and then dried using N₂ gas. Ti/Au contacts were deposited by e-beam evaporation on part of the front and back sides of each sample. These were then annealed at 450°C in N₂ for 30 min to improve their contact resistance. Even on low-resistivity Sn-doped β -Ga₂O₃

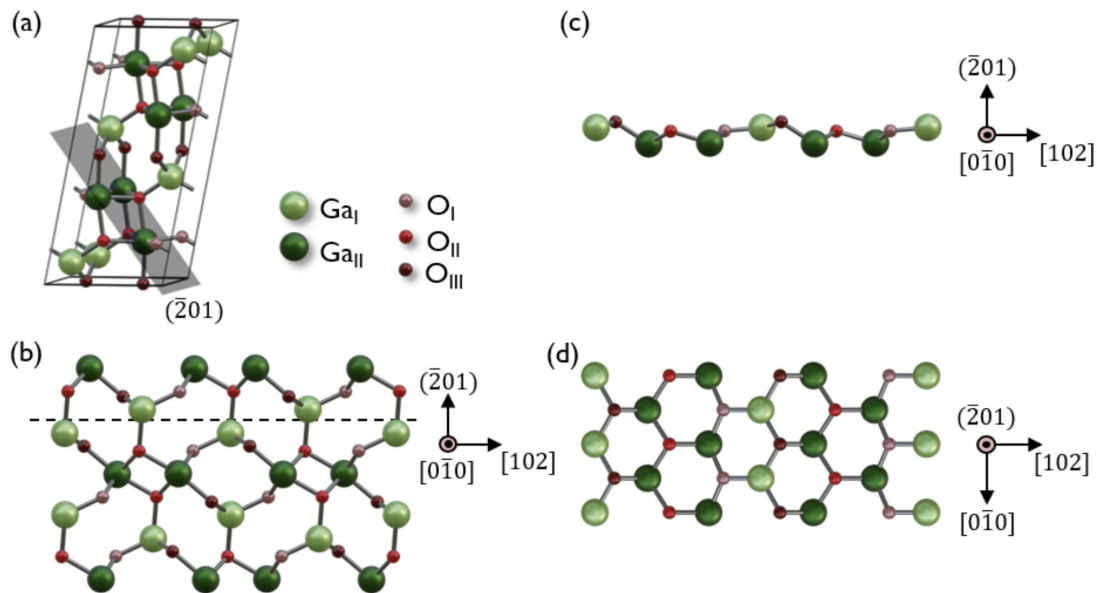


FIG. 1. (a) β - Ga_2O_3 unit cell (20 atoms) comprising two Ga sites: Ga_I (fourfold coordinated) and Ga_{II} (sixfold coordinated), and three O sites: O_I (onefold coordinated to Ga_I and twofold coordinated to Ga_{II} atoms), O_{II} (onefold coordinated to Ga_I and threefold coordinated to Ga_{II} atoms), and O_{III} (twofold coordinated to Ga_I atoms and onefold coordinated to Ga_{II}); (b) β - Ga_2O_3 crystal projection with the $[0\bar{1}0]$ direction perpendicular to the page with the dashed line in (b) indicating the cleavage plane used to create the (c) lateral and (d) top projections of the relaxed $(\bar{2}01)$ surface. Orthogonal crystallographic vectors $[0\bar{1}0]$, $[102]$ and the direction normal to the $(\bar{2}01)$ plane are included to help visualize the projections. The coordinates for the relaxed $(\bar{2}01)$ surface were taken from Ref. [32].

substrates, annealed Ti/Au contacts were necessary to provide adequate grounding to the spectrometer to eliminate sample charging during XPS.

These samples were then subjected to different surface treatments, involving immersion in aqueous NaOH and H_2SO_4 solutions and annealing (600°C) in wet O_2 . The following nomenclature is adopted for sample identification: “As-received” samples were only cleaned in the organic solvents described above; “wet O_2 annealed” samples were annealed at 600°C for 30 min in wet oxygen (i.e. O_2 gas bubbled through deionized H_2O); “NaOH-treated” samples were immersed in 1 M aqueous NaOH at 60°C for 30 min; “ H_2SO_4 -treated” samples were immersed in 1 M aqueous NaOH at 60°C for 30 min followed by concentrated ($\sim 95\%$) H_2SO_4 at RT for 10 min. Atomic force microscope images taken with a Digital Instruments Dimension 3100 instrument showed no significant change in the morphology of the $(\bar{2}01)$ β - Ga_2O_3 surface following these treatments, with the exception of the H_2SO_4 -treated sample in which the surface atomic-step terrace structure became more visible (see Supplemental Material Fig. S2 [34]).

B. Core-level and valence-band synchrotron XPS

Surface-sensitive, variable photon energy ($h\nu = 1267$ to 150 eV) XPS measurements were performed at the soft x-ray beamline of the Australian Synchrotron on the as-received and surface-treated β - Ga_2O_3 $(\bar{2}01)$ samples. Spectra were recorded on samples *as loaded* and after ~ 15 -min *in situ* heating steps at 100°C increments from RT to 600°C . All XPS spectra were measured at RT at a base pressure of $< 2 \times 10^{-10}$ mbar, with the heating steps performed in a

separate UHV preparation chamber (base pressure $\sim 5 \times 10^{-10}$ mbar at RT, temporarily rising to $\sim 10^{-7}$ mbar during the 600°C heating cycle). Each sample was electrically grounded to the spectrometer via a tantalum foil sample holder that was connected to the front- and back-side annealed Ti/Au Ohmic contacts. This was necessary to avoid sample charging and allowed the Fermi level of each sample to be directly referenced to the zero of the XPS spectrometer BE scale. The absence of sample charging was confirmed by the lack of any BE shifts in the measured core-level and VB spectra on varying the incident photon flux.

The spectrometer BE scale was calibrated at each photon energy using the Au $4f$ core-level doublet and the Fermi edge of a clean gold reference foil. The uncertainty in the measured binding energies was ± 0.04 eV. Spectra were collected using a Specs Phoibos 150 hemispherical electron energy analyzer with the detector axis positioned normal to the sample surface. The incident x-ray photon energy ($h\nu$) was varied between VB and core-level scans to maintain the same surface sensitivity, i.e., the same photoelectron kinetic energy (~ 150 eV) and inelastic mean-free path λ of ~ 6.2 Å (using the TPP-2M formula) [35]. Consequently, O $1s$ and Ga $2p$ core-level spectra were collected at 680 and 1267 eV, respectively, with VB spectra taken at $h\nu = 150$ eV. Survey spectra were measured on each sample at $h\nu = 1267$ eV to check for surface contaminants, including adventitious carbon which remained below detectable levels.

The hydroxyl coverage was estimated using the relative component areas of O $1s$ core-level spectra, fitted using pseudo-Voigt functions on a Shirley background, with the full width at half maximum (FWHM) constrained to < 2 eV. The VB spectra were fitted in a similar way (FWHM < 2.4 eV).

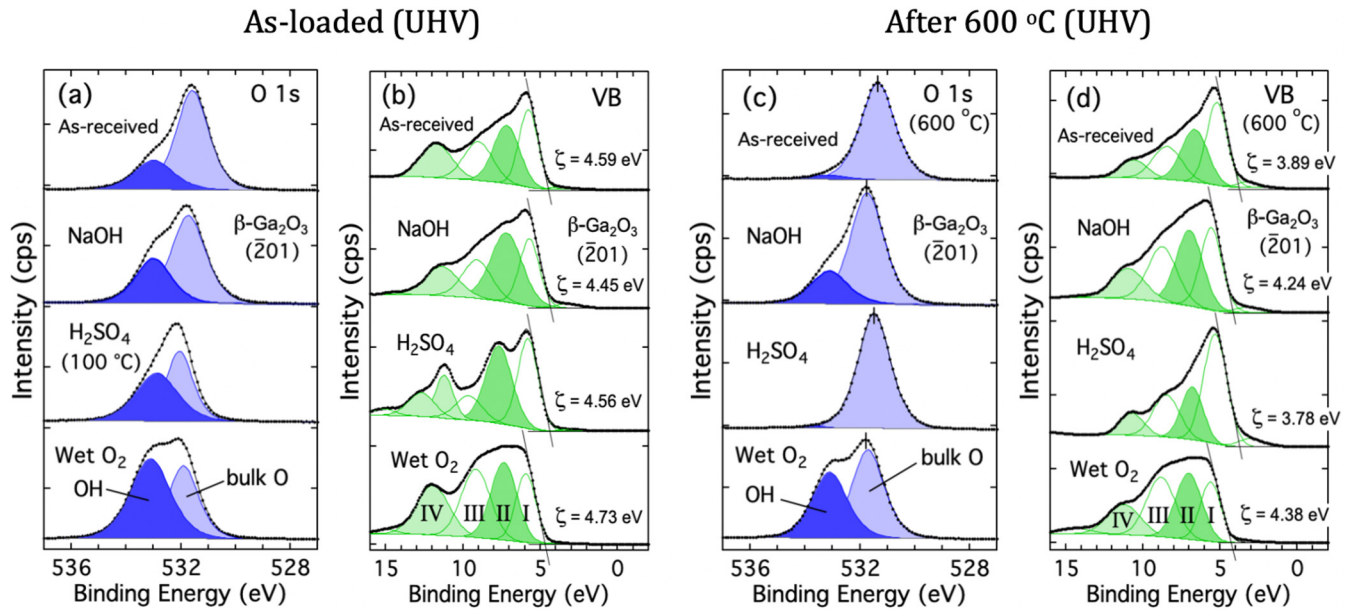


FIG. 2. (a), (c) O 1s core-level spectra ($h\nu = 680$ eV) and (b), (d) valence-band spectra ($h\nu = 150$ eV) measured at RT on as-received, NaOH-treated, H₂SO₄-treated, and wet O₂ annealed β -Ga₂O₃($\bar{2}01$) surfaces: (a) and (b) as loaded (i.e., before heating) and (c) and (d) after *in situ* heating to 600 °C. [Note: (1) the main component peaks in the VB spectra have been labelled I, II, III, IV; (2) the spectra for the H₂SO₄-treated sample in Figs 2(a) and 2(b) were measured at RT after *in situ* heating at 100 °C.]

The near-surface band bending (V_{bb}) at a depth of ~ 6.2 Å below the surface was determined from the ($h\nu = 150$ eV) VB spectra using Eq. (1), as described previously in Sec. I. In this work, we have used the standard linear VB-edge extrapolation method to determine the parameter ζ used in Eq. (1). This allows comparisons with many previous band-bending studies on oxide semiconductors, including β -Ga₂O₃, ZnO, SnO₂, and In₂O₃, that have used the same method [6,7,9,13,14,22,23]. A significant part of our study involves the *changes* in band bending (ΔV_{bb}) produced by surface treatments that alter the nature and stability of the OH termination of the ($\bar{2}01$) β -Ga₂O₃ surface, and this is independent of the method used to determine ζ . However, we will also examine the implications of the choice of method in establishing the electronic nature of bare and hydroxylated β -Ga₂O₃ surfaces.

III. RESULTS

A. As-loaded samples

Figures 2(a) and 2(b) show O 1s spectra ($h\nu = 680$ eV) and VB spectra ($h\nu = 150$ eV) measured at RT for the β -Ga₂O₃($\bar{2}01$) surface in its as-received state, and after NaOH, H₂SO₄, and wet O₂ (600 °C) surface treatments. These spectra were recorded as loaded before any *in situ* heating, with the exception of the H₂SO₄-treated sample for which the spectrum recorded after heating at 100 °C is shown. This is because survey spectra ($h\nu = 1267$ eV) from the as-loaded H₂SO₄-treated sample (not shown) revealed a small SO₄-related S $2p_{3/2}$ peak (BE = 168 eV) that disappeared after heating, suggesting that some weakly attached residual H₂SO₄ was present on the as-loaded H₂SO₄-treated sample. This is also the only sample for which the as-loaded condition did not correspond to the highest measured value of ζ and therefore

the lowest V_{bb} [see Fig. 3(j)]. The lowest V_{bb} for the H₂SO₄-treated sample was observed after 100 °C heating, possibly due to the removal of the residual H₂SO₄ (note: the O 1s and VB spectra for the as-loaded H₂SO₄-treated sample are shown in the Supplemental Material Fig. S3 [34]).

The O 1s spectra for each sample in Fig. 2(a) could be fitted with just two components: a low BE peak due to bulk oxygen and a higher BE peak due to oxygen atoms in surface-terminating OH groups, with the relative area of the surface OH component given in Table I. The surface nature of the OH component was confirmed by observing that its intensity rapidly decreased with increasing x-ray photon energy (see Supplemental Material Fig. S4 [34]). Surface OH groups are most likely formed by the dissociative adsorption of H₂O on the bare β -Ga₂O₃ surface on exposure to atmosphere, with OH binding to surface Ga atoms (Ga_s) via the oxygen water atom (O_w) to form Ga_s-O_wH_w, and H binding to surface oxygen atoms (O_s) to form O_s-H_w [32,36,37]. The key difference between these OH groups is the coordination of the O atom: for Ga_s-O_wH_w the O_w atom is coordinated to a single Ga atom, whereas in O_s-H_w the O_s atom is bonded to three surface Ga atoms. However, it was not possible to unambiguously distinguish between these different OH environments in the O 1s spectra. This is similar to the case for ZnO where no significant difference was observed in the BE separation of the OH and bulk O components in O 1s spectra taken from the hydroxylated Zn-polar (0001) and O-polar (000 $\bar{1}$) faces, on which Zn_s-O_wH_w (O_w bonded to one Zn atom) and O_s-H_w (O_s bonded to three Zn atoms) are the dominant OH species, respectively [13,38].

All three surface treatments resulted in an increase in the relative area of the surface OH component (A_{OH}) as shown in Table I, suggesting an increase in the surface density of the OH termination, with wet O₂ (600 °C) annealing producing

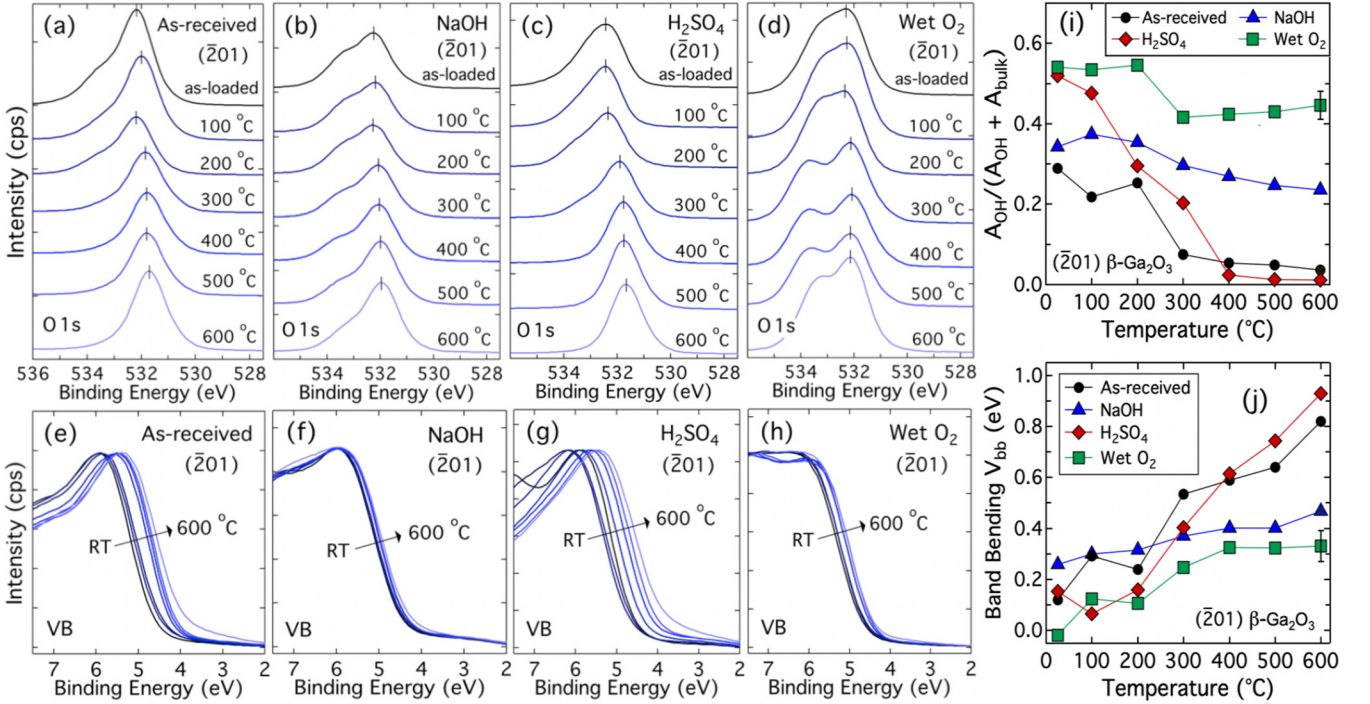


FIG. 3. (a)–(d) O $1s$ core-level spectra ($h\nu = 680$ eV) and (e)–(h) valence band spectra ($h\nu = 150$ eV) taken on (a), (e) as-received, (b), (f) NaOH-treated, (c), (g) H_2SO_4 -treated, and (d), (h) wet O_2 annealed $(\bar{2}01)\beta\text{-Ga}_2\text{O}_3$ samples, after successive ~ 15 -min heating steps from RT to 600°C . Panels (i) and (j) show the extracted values of the OH area fraction A_{OH} and surface band bending V_{bb} after each temperature step, with an indicative error bar provided in each panel.

the strongest effect. It is likely that (i) NaOH (i.e., high- $p\text{H}$) treatment increases the relative density of surface $\text{Ga}_s\text{-O}_w\text{H}_w$ species, and (ii) H_2SO_4 (low- $p\text{H}$) treatment increases the relative density of $\text{O}_s\text{-H}_w$, while (iii) 600°C wet O_2 annealing (neutral $p\text{H}$) equally increases the surface density of $\text{Ga}_s\text{-O}_w\text{H}_w$ and $\text{O}_s\text{-H}_w$, due to an increase in dissociative adsorption. It is also possible that these aqueous treatments will cause an increase in molecular H_2O , possibly in the form of additional physisorbed layers. However, there is no indication of a separate H_2O component, as observed in the case of ZnO and In_2O_3 [13,39], in any of the O $1s$ spectra, although it is possible that this cannot be separately resolved in the case of $\beta\text{-Ga}_2\text{O}_3$.

Significant changes were also observed in the structure of the VB spectra following the different surface treatments:

this is shown in Fig. 2(b) where the lowest BE emission at ~ 5.5 eV is due to $\text{O}2p$ derived states and the higher BE components still mainly involve $\text{O}2p$ states but with small Ga $4s$, $4p$, and $3d$ contributions [40]. Each of VB spectra were fitted with four main component peaks that are labeled I to IV in Fig. 2(b). These VB spectra are composed of intrinsic DOS and contributions arising from the hydroxyl termination of the surface, with the latter mainly involving peak II (~ 7 eV) and peak IV (~ 12 eV). Emission at these energies are partially shaded in Fig. 2(b) and their respective areas are shown as percentages of the total VB area in Table I. Zhou *et al.* [36] used DFT calculations to determine the partial DOS (PDOS) for the dissociative adsorption of H_2O on the (001) surface of $\alpha\text{-Ga}_2\text{O}_3$ and found distinct PDOS contributions for $\text{Ga}_s\text{-O}_w\text{H}_w$ and $\text{O}_s\text{-H}_w$ species, arising from

TABLE I. Extracted synchrotron XPS parameters as loaded (i.e., before) and after *in situ* 600°C heating for the as-received, NaOH-treated, H_2SO_4 -treated, and wet O_2 annealed $\beta\text{-Ga}_2\text{O}_3(\bar{2}01)$ samples: area fraction (A_{OH}) of the OH component in the O $1s$ spectrum; E_V to E_F separation parameter (ζ); surface band bending (V_{bb}); the change in band bending (ΔV_{bb}) relative to the as-received sample and also (last column) between samples after 600°C heating; and the areas [$A_{\text{II}}(A_{\text{IV}})$] of peak II (and peak IV) as percentages of the total VB area. [Note: V_{bb} and ΔV_{bb} were determined using Eq. (1) with $E_g = 4.71$ eV.]

Surface treatment	As loaded					After 600°C					ΔV_{bb}
	A_{OH}	ζ (eV)	V_{bb} (eV)	ΔV_{bb} (eV)	$A_{\text{II}}(A_{\text{IV}})$ (%)	A_{OH}	ζ (eV)	V_{bb} (eV)	ΔV_{bb} (eV)	$A_{\text{II}}(A_{\text{IV}})$ (%)	After 600°C
As received	0.289	4.59	+0.12	0.00	29(21)	0.036	3.89	+0.82	0.00	30(11)	+0.70
NaOH	0.343	4.45	+0.26	+0.14	38(17)	0.235	4.24	+0.47	-0.35	30(15)	+0.21
H_2SO_4 (100°C)	0.520	4.64	+0.07	-0.05	32(19)	0.011	3.78	+0.93	+0.11	21(10)	+0.86
Wet O_2 Anneal	0.541	4.73	-0.02	-0.14	29(23)	0.446	4.38	+0.33	-0.49	30(17)	+0.35

the different Ga coordination of the respective O atoms, with the $\text{Ga}_s\text{-O}_w\text{H}_w$ -related PDOS occurring at lower binding energy. This assignment is consistent with the increase in peak II (~ 7 eV) emission (associated with $\text{Ga}_s\text{-O}_w\text{H}_w$) and the decrease in peak IV (~ 12 eV) emission (associated with $\text{O}_s\text{-H}_w$) for the NaOH-treated sample. The most noticeable change in the wet O_2 annealed sample was a significant increase of the relative intensities of peaks II and IV, and also peak III, compared to peak I. This is not surprising as wet O_2 annealing is expected to increase the surface density of both $\text{Ga}_s\text{-O}_w\text{H}_w$ and $\text{O}_s\text{-H}_w$. The H_2SO_4 -treated sample showed a more complicated change with a positional shift (to lower BE) and decrease in the FWHM of the $\text{O}_s\text{-H}_w$ -related peak IV emission near ~ 12 eV and the appearance of an additional related peak that is not yet understood.

Table I shows the values of ζ and V_{bb} determined from the VB spectra using Eq. (1), with ζ obtained using the standard linear VB-edge extrapolation method [29]. In the case of the moderately doped $\beta\text{-Ga}_2\text{O}_3$ material used in this study, Eq. (1) simplifies to $V_{bb} \approx E_g - \zeta$, as $\xi = kT/q \ln(N_C/n) \approx 0$ because $n \approx N_C$. We will focus on the changes in band bending ΔV_{bb} relative to the as-received surface and discuss the absolute values later. Both H_2SO_4 treatment ($\Delta V_{bb} = -0.05$ eV) and wet O_2 annealing ($\Delta V_{bb} = -0.14$ eV) produced downward shifts in band bending, with wet O_2 annealing producing the strongest effect. In contrast, NaOH treatment produced an upward shift in band bending ($\Delta V_{bb} = +0.14$ eV). The direction of these changes were consistently observed in several other $\beta\text{-Ga}_2\text{O}_3$ samples. They are also consistent with DFT simulations of H_2O dissociation on the $\beta\text{-Ga}_2\text{O}_3$ ($\bar{2}01$) surface by Anvari *et al.* [32], who used Bader charge analysis to show that a significant net negative charge is transferred to the surface by dissociated H_2O , with electronic charge transferred to the surface by $\text{O}_s\text{-H}_w$ species and (to a weaker extent) away from the surface by $\text{Ga}_s\text{-O}_w\text{H}_w$. This is consistent with the increase in V_{bb} after NaOH treatment that increases the relative concentration of $\text{Ga}_s\text{-O}_w\text{H}_w$ (and therefore reduces the electron density at the surface) and the corresponding decrease in V_{bb} after H_2SO_4 treatment that increases the relative concentration of $\text{O}_s\text{-H}_w$ (and therefore increases the electron density at the surface). Wet O_2 annealing, that is expected to equally increase the surface density of $\text{Ga}_s\text{-O}_w\text{H}_w$ and $\text{O}_s\text{-H}_w$, also decreases V_{bb} since the electron-donating effect of $\text{O}_s\text{-H}_w$ is predicted to be stronger than the electron-withdrawing effect of $\text{Ga}_s\text{-O}_w\text{H}_w$ [32].

B. After *in situ* heating

Figure 3 shows the O 1s spectra [3(a)–3(d)], the low-BE edge of the VB spectra [3(e)–3(h)], and the extracted values of the OH area fraction A_{OH} [3(i)] and the surface band bending V_{bb} [3(j)], after *in situ* heating the as-received and surface-treated $\beta\text{-Ga}_2\text{O}_3$ ($\bar{2}01$) samples from RT to 600°C , in 100°C steps. Figures 2(c) and 2(d) also show the O 1s and VB spectra after 600°C heating in greater detail, with individual components fitted in the same way as before. It is clear that significant differences in the thermal stability of the hydroxyl termination A_{OH} and the band bending V_{bb} were produced by the different surface treatments. The OH coverage of the as-received and, in particular, the H_2SO_4 -treated sample could be

almost entirely removed by 600°C UHV heating, producing an almost “bare” (OH-free) surface. This was accompanied by a large upward shift in band bending of $+0.70$ and $+0.86$ eV for the as-received and H_2SO_4 -treated samples, respectively.

It is also clear that both NaOH treatment and wet O_2 annealing were effective at both stabilizing the OH termination against thermal desorption and reducing the increase in V_{bb} after *in situ* heating. In addition to the results shown here, the wet O_2 annealed sample was also heated to 750°C for ~ 2 h without any significant changes in A_{OH} or V_{bb} relative to the minor changes measured after 600°C . This highlights the very high thermal stability of the surface OH termination produced by wet O_2 annealing.

C. After *in situ* H_2O dosing and atmospheric exposure

To further explore the relationship between the surface OH coverage A_{OH} and band bending V_{bb} , a series of additional *in situ* experiments were performed on the as-received and surface-treated $\beta\text{-Ga}_2\text{O}_3$ ($\bar{2}01$) samples. Following the first UHV heating cycle to 600°C (shown in Fig. 3), the samples were subsequently: (1) *in situ* exposed at RT to 25 000 langmuir (L) of degassed H_2O at a pressure of 10^{-4} mbar (for ~ 4 min); (2) *in situ* reheated to 600°C (for ~ 15 min); and (3) exposed to atmosphere (for ~ 30 min). Figures 4(a)–4(h) show the evolution of the O 1s spectra and the VB edge following these additional experiments, while Figs. 4(i) and 4(j) show the extracted values of A_{OH} and V_{bb} after each step. The results are also numerically tabulated in Table II, with the as-loaded and first *in situ* 600°C heating results included for comparison. For each sample, *in situ* 25 000 L H_2O dosing caused A_{OH} to return to similar levels to those measured in the as-loaded samples before heating. Surprisingly, in each case only a partial corresponding recovery in V_{bb} towards the as-loaded values was observed. The changes in A_{OH} and V_{bb} for the NaOH-treated and wet O_2 annealed samples were significantly smaller due to the much stronger thermal stability of their OH coverage. Therefore, we will focus on the as-received and H_2SO_4 -treated samples for which significantly larger changes in A_{OH} and V_{bb} were observed: Although 25 000 L H_2O dosing restored A_{OH} to close to the as-loaded values, there was only an accompanying $\sim 30\%$ recovery in V_{bb} for the as-received and H_2SO_4 -treated samples. The second 600°C heat treatment again produced an almost complete removal of the OH signal and an increase in V_{bb} to similar values to those produced by the first 600°C heating cycle. In fact, V_{bb} was slightly larger after the second 600°C heat treatment, due to a more complete removal of the OH termination. Surprisingly, atmospheric exposure produced an even smaller recovery in V_{bb} than *in situ* 25 000 L H_2O dosing, i.e., only $\sim 11\%$ ($\sim 19\%$) for the as-received (H_2SO_4 -treated) samples. This is in contrast to similar experiments carried out on the nonpolar ($10\bar{1}0$) and O-polar ($000\bar{1}$) surfaces of ZnO for which an almost fully reversible recovery in both A_{OH} and V_{bb} was observed after atmosphere exposure [13,14]. Since atmospheric exposure represents a significantly larger H_2O exposure than *in situ* 25 000 L H_2O dosing, it seems likely that the presence of atmospheric O_2 and/or N_2 slows the adsorption and dissociation of H_2O on $\beta\text{-Ga}_2\text{O}_3$ ($\bar{2}01$) surfaces. Berthold *et al.* [21] have observed a similar

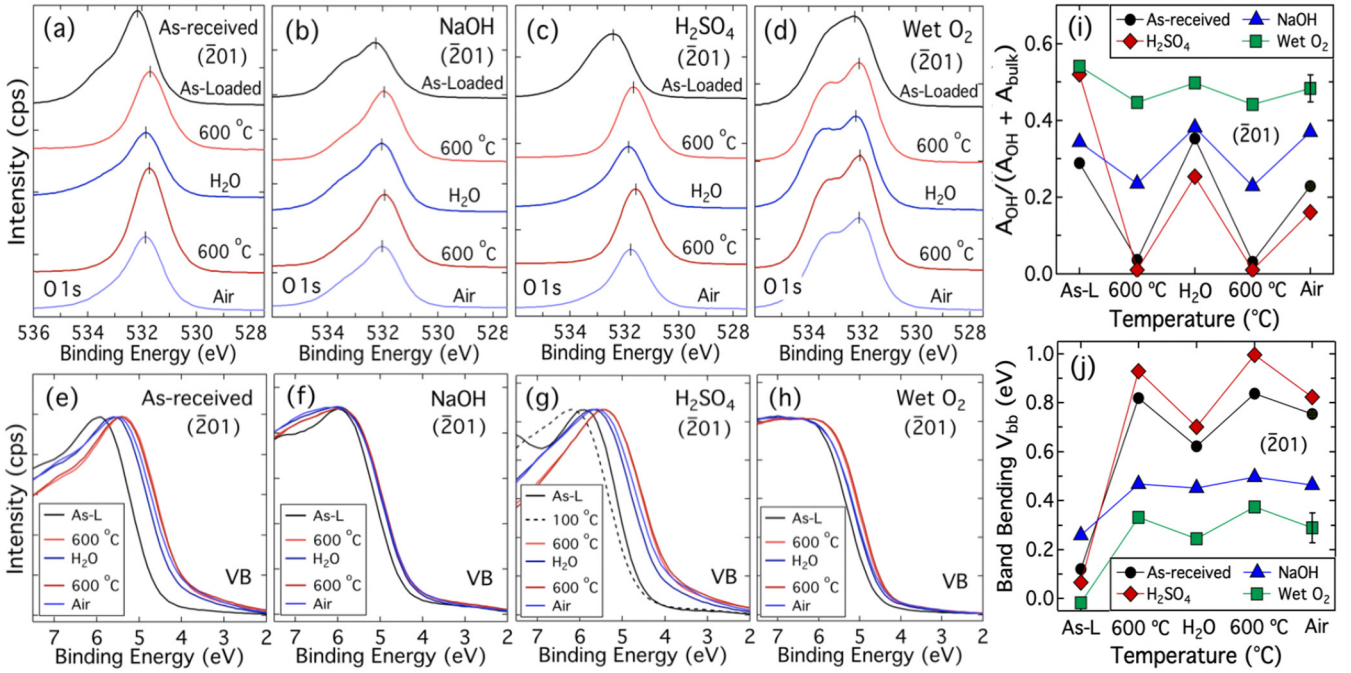


FIG. 4. (a)–(d) O $1s$ core-level spectra ($h\nu = 680$ eV) and (e)–(h) valence band spectra ($h\nu = 150$ eV) measured on (a), (e) as-received, (b), (f) NaOH-treated, (c), (g) H_2SO_4 -treated (100°C), and (d), (h) wet O_2 annealed $\beta\text{-Ga}_2\text{O}_3(\bar{2}01)$ samples, after each of the following consecutive treatments: (i) as-loaded (As-L), (ii) ~ 15 min 600°C , (iii) 25 000 L H_2O dosing, (iv) ~ 15 min 600°C , (v) exposure to atmosphere (air) for ~ 30 min. Panels (i) and (j) show the extracted values of the OH area fraction A_{OH} and band bending V_{bb} after each experiment, with an indicative error bar provided in each panel.

competition between O_2 , O_3 , and H_2O for surface adsorption sites on $\text{In}_2\text{O}_3(111)$ surfaces. Finally, an examination of Table II across all samples shows that the difference in V_{bb} between the least and most hydroxylated ($\bar{2}01$) surfaces was $+1.02$ eV, illustrating the large electronic effect of the hydroxyl termination on ($\bar{2}01$) $\beta\text{-Ga}_2\text{O}_3$ surfaces.

IV. DISCUSSION

Surface-sensitive synchrotron XPS spectroscopy ($\lambda \sim 6.2$ Å) was used to explore the stability of the hydroxyl termination and electronic band bending V_{bb} at the as-received ($\bar{2}01$) surfaces of high-quality $\beta\text{-Ga}_2\text{O}_3$ single crystals and those subjected to different surface treatments. The key findings were:

(1) All as-received ($\bar{2}01$) surfaces were hydroxyl terminated, with a significant surface OH component consistently observed in their O $1s$ spectra. Removal of this OH termina-

tion consistently produced a large upward shift in V_{bb} of up to 1.0 eV;

(2) NaOH treatment of as-received ($\bar{2}01$) surfaces consistently produced an upward shift in V_{bb} , while H_2SO_4 treatment and wet O_2 annealing (at 600°C) both produced downward shifts in V_{bb} ;

(3) NaOH treatment and wet O_2 annealing both produced a strong increase in the thermal stability of the surface OH coverage. In contrast, the stability of the OH coverage was reduced following H_2SO_4 treatment;

(4) *In situ* H_2O dosing of bare ($\bar{2}01$) surfaces produced only a partial ($\sim 30\%$) recovery in V_{bb} , compared to as-received surfaces. Atmosphere exposure (~ 15 min) produced a significantly smaller ($\sim 10\text{--}20\%$) recovery in V_{bb} .

These findings can be explained by differences in the electron-donating nature of different OH species and the stabilization of the OH termination at high coverages by hydrogen bonding. Hydroxylation of the bare (OH-free) $\beta\text{-Ga}_2\text{O}_3(\bar{2}01)$

TABLE II. Area fraction (A_{OH}) of the OH component and surface band bending (V_{bb}) from synchrotron XPS for as-received, NaOH-treated, H_2SO_4 -treated, and wet O_2 annealed $\beta\text{-Ga}_2\text{O}_3(\bar{2}01)$ samples after the following sequential experiments: (i) as loaded, (ii) first 600°C heating, (iii) 25 000 L *in situ* H_2O dosing, (iv) second 600°C heating, and (v) atmospheric (i.e., air) exposure.

Surface treatment	As loaded		1 st 600°C		25 000 L H_2O		2 nd 600°C		Air exposure	
	A_{OH}	V_{bb} (eV)	A_{OH}	V_{bb} (eV)	A_{OH}	V_{bb} (eV)	A_{OH}	V_{bb} (eV)	A_{OH}	V_{bb} (eV)
As received	0.289	+0.12	0.036	+0.82	0.352	+0.62	0.031	+0.84	0.229	+0.75
NaOH	0.343	+0.26	0.235	+0.47	0.381	+0.45	0.229	+0.50	0.369	+0.46
H_2SO_4 (100°C)	0.520	+0.07	0.011	+0.93	0.253	+0.70	0.010	+1.00	0.161	+0.82
Wet O_2 anneal	0.541	-0.02	0.446	+0.33	0.498	+0.24	0.442	+0.37	0.483	+0.29

surface is predicted to occur via the fast exothermic molecular adsorption of H_2O in which the water oxygen atom (O_w) attaches to a Ga_s site, forming $\text{Ga}_s\text{-O}_w\text{H}_2$, followed by a relatively slow dissociation process that forms two different hydroxyl species, i.e., $\text{Ga}_s\text{-O}_w\text{H}_w + \text{O}_s\text{-H}_w$ [32,36,37]. The fast molecular adsorption of H_2O followed by a slower OH.H dissociation has been observed by Giber *et al.* [41] on rf-sputtered $\beta\text{-Ga}_2\text{O}_3$ thin films. Anvari *et al.* [32] used DFT Bader charge analysis to show that H_2O in both molecular and dissociatively adsorbed forms acts as a Lewis base transferring electronic charge to the $\beta\text{-Ga}_2\text{O}_3$ ($\bar{2}01$) surface, with dissociated H_2O producing a significantly stronger donor effect. This is due to dissociated water (OH.H) binding to surface Ga_s and O_s sites as $\text{Ga}_s\text{-O}_w\text{H}_w$ and $\text{O}_s\text{-H}_w$, with the latter transferring a relatively large amount of electronic charge to the surface which dominates the smaller charge-withdrawing effect of $\text{Ga}_s\text{-O}_w\text{H}_w$ [32]. Consequently, increasing H_2O dissociation will result in a net increase in surface donor density, and an increasing downward shift in V_{bb} . In addition, surface treatments that increase the concentration of $\text{O}_s\text{-H}_w$ relative to $\text{Ga}_s\text{-O}_w\text{H}_w$ will also increase the surface electron density and the downward shift in V_{bb} . This explains the observation that although all three surface treatments increased the surface OH component (A_{OH}) in the $\text{O } 1s$ spectra, H_2SO_4 treatment (that is likely to increase $\text{O}_s\text{-H}_w$) and wet O_2 annealing (that should equally increase both $\text{O}_s\text{-H}_w$ and $\text{Ga}_s\text{-O}_w\text{H}_w$) produced downward shifts in V_{bb} , while NaOH treatment (that is likely to increase $\text{Ga}_s\text{-O}_w\text{H}_w$) produced an upward shift in V_{bb} , compared to as-received samples.

The slow dissociation of molecularly adsorbed H_2O and the strong electron-donating nature of $\text{O}_s\text{-H}_w$ explains the difference in band bending between as-received ($\bar{2}01$) $\beta\text{-Ga}_2\text{O}_3$ surfaces and *in situ* prepared bare surfaces that were subsequently dosed with H_2O . The former were characterized by a significantly larger downward shift in V_{bb} compared to bare surfaces since they have been exposed to atmospheric H_2O for a much longer period of time (i.e., many weeks), leading to an increased density of dissociated $\text{O}_s\text{-H}_w$ and $\text{Ga}_s\text{-O}_w\text{H}_w$ species. The smaller ($\sim 30\%$) downward shift in V_{bb} on bare ($\bar{2}01$) surfaces following *in situ* H_2O dosing is a result of a much shorter exposure (only ~ 4 min) to H_2O . The even smaller ($\sim 10\text{--}20\%$) change in V_{bb} on exposing the bare ($\bar{2}01$) surface to atmosphere (~ 30 min) is surprising and may be due to a competition for surface adsorption sites between electron-withdrawing O_2 and electron-donating H_2O molecules. This competition is known to occur in $\beta\text{-Ga}_2\text{O}_3$ gas sensors and catalysts [42], where the formation of surface OH groups significantly reduces the sensitivity to CO and O_2 , while a similar effect has also been observed on $\text{In}_2\text{O}_3(111)$ surfaces [21].

The change in the stability of the OH coverage following different surface treatments is likely to be related to the hydrogen-bonding density at the surface, although differences in the OH bond strength in the $\text{O}_s\text{-H}_w$ and $\text{Ga}_s\text{-O}_w\text{H}_w$ environments may also play a role. Hydrogen bonding is known to stabilize the hydroxyl termination of $\text{ZnO}(10\bar{1}0)$ and $\text{SnO}_2(100)$ surfaces, on which closed hydrogen-bonded networks of OH groups can form at close to monolayer coverages [43–45].

We therefore first consider the effect of hydrogen bonding: there are multiple hydrogen-bonding opportunities for both

molecular- and dissociatively adsorbed H_2O species, both with each other and with the $\beta\text{-Ga}_2\text{O}_3$ surface. Figure 5 shows a model for the hydroxylation of the relaxed $\beta\text{-Ga}_2\text{O}_3$ ($\bar{2}01$) surface in which we assume that H_2O preferentially adsorbs onto (i) Ga_I sites and (ii) Ga_{II} sites that are adjacent to two O_{II} atoms. These are likely to be the most chemically active sites since the ($\bar{2}01$) surface is formed by breaking only $\text{Ga}_I\text{-O}_{II}$ bonds. However, the following arguments equally apply to surfaces in which H_2O molecules adsorb onto all surface Ga atoms.

During molecular adsorption [Fig. 5(a)], the dipole of the adsorbed H_2O molecule is predicted to lie almost parallel to the surface [32,36], which promotes the hydrogen bonding of water H atoms with adjacent surface O_s atoms, while for dissociatively adsorbed water (OH.H), hydrogen bonding can occur between dissociated $\text{Ga}_s\text{-O}_w\text{H}_w$ and $\text{O}_s\text{-H}_w$ groups, with the number of possible interactions increasing with OH coverage [Fig. 5(b)]. Hydrogen bonding is therefore likely to stabilize the OH termination of the ($\bar{2}01$) surface as the dissociated water (OH.H) coverage increases, which explains the strong thermal stability following wet O_2 annealing. Hydrogen bonding can also occur between $\text{Ga}_s\text{-O}_w\text{H}_w$ and surface O_s atoms. Zhou *et al.* [36] used DFT to show that the distance between $\text{Ga}_s\text{-O}_w\text{H}_w$ groups and O_s atoms on $\alpha\text{-Ga}_2\text{O}_3(110)$ surfaces is significantly reduced by the corrugated nature of the surface, allowing strong hydrogen bonds to form. A similar corrugated surface structure is likely to be present on the $\beta\text{-Ga}_2\text{O}_3$ ($\bar{2}01$) surface [32]. Consequently, NaOH treatment is also likely to increase the stability of the OH coverage due to an increase of the relative surface density of $\text{Ga}_s\text{-O}_w\text{H}_w$ species that can form hydrogen bonds with O_s sites [Fig. 5(c)]. Conversely, H_2SO_4 treatment is likely to remove $\text{Ga}_s\text{-O}_w\text{H}_w$ and increase the relative surface density of $\text{O}_s\text{-H}_w$, which explains the decrease in thermal stability of the OH coverage, since there are no hydrogen-bonding opportunities between adjacent $\text{O}_s\text{-H}$ species or between $\text{O}_s\text{-H}$ species and any surface atoms [Fig. 5(d)]. Although the model shown in Fig. 5 is idealized in that it shows complete $\text{O}_s\text{-H}_w$ ($\text{Ga}_s\text{-O}_w\text{H}_w$) removal following NaOH (H_2SO_4) treatment, it is consistent with the overall changes in band bending and thermal stability following the different surface treatments.

We now consider the effect of differences in the bond strength of the different OH species: it is possible that the thermal stability of the $\text{Ga}_s\text{-O}_w\text{H}_w$ bond is higher than that of the $\text{O}_s\text{-H}_w$ bond, although this has not been addressed in any of the DFT studies on $\beta\text{-Ga}_2\text{O}_3$ surfaces [32,36,37]. However, in the case of ZnO , Heinhold *et al.* [13,14] observed a much higher thermal stability for OH groups on the Zn-polar (0001) face, on which $\text{Zn}_s\text{-O}_w\text{H}$ is likely to be the dominant OH species, compared to the O-polar (000 $\bar{1}$) face, where $\text{O}_s\text{-H}$ is likely to be the dominant species. A higher thermal stability for $\text{Ga}_s\text{-O}_w\text{H}_w$ species could also explain the increased thermal stability of the hydroxyl coverage following NaOH and wet O_2 annealing treatments, and why the most complete hydroxyl removal was achieved on H_2SO_4 -treated surfaces.

The relative concentrations of the different OH species (i.e., $\text{O}_s\text{-H}$, $\text{Ga}_s\text{-O}_w\text{H}$, and $\text{Ga}_s\text{-O}_w\text{H}_2$) and their different relative contributions to the surface electron density (i.e., strong donor, weak acceptor, and weak donor, respectively

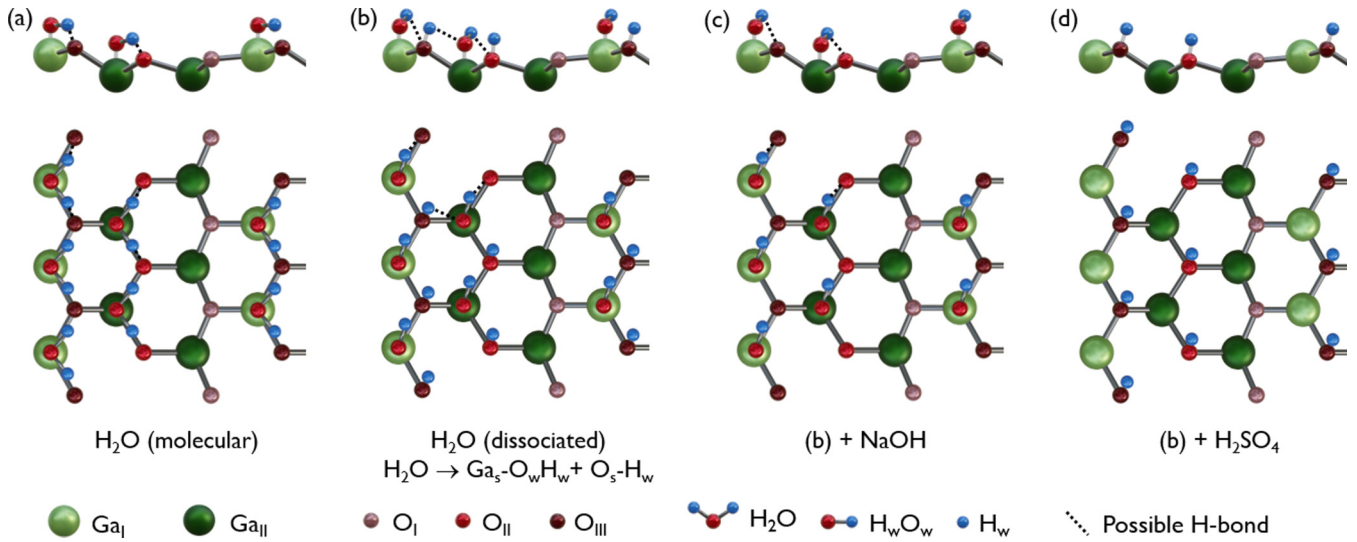


FIG. 5. Model of the hydroxylation of bare β -Ga₂O₃($\bar{2}01$) surfaces: (a) molecular H₂O adsorption, (b) dissociative H₂O adsorption, (c) NaOH treatment, (d) H₂SO₄ treatment. (Note: the coordinates for the relaxed ($\bar{2}01$) surface were taken from Ref. [32].)

[32]) may also explain the nonlinear relationship between the surface OH coverage (A_{OH}) and V_{bb} . This is shown in Fig. 6 in which V_{bb} is plotted against A_{OH} for all the as-received and surface-treated ($\bar{2}01$) β -Ga₂O₃ samples during the first 600 °C heating cycle. It is clear that the effect of OH coverage on V_{bb} is greatest at low coverages, with small changes in A_{OH} producing large variations in V_{bb} . At larger coverages this effect tends to saturate, most likely as the OH coverage approaches a complete monolayer. In the case of ZnO (10 $\bar{1}0$) and SnO₂ (100) surfaces, monolayer OH coverages can lead to the formation of closed networks of strongly hydrogen-bonded OH groups onto which additional H₂O molecules can

only weakly physisorb [43–45]. Further theoretical studies are required to examine the question of whether similar closed networks can form on β -Ga₂O₃ surfaces.

Thus far, we have focused on the changes in band bending (ΔV_{bb}) produced by different surface treatments that modify the nature and stability of the native OH termination of the ($\bar{2}01$) β -Ga₂O₃ surface. We now discuss the absolute values of V_{bb} for different surface conditions and the implications for the electronic nature of the ($\bar{2}01$) surface, i.e., electron depletion or electron accumulation. Absolute values of V_{bb} depend on the choice of method used to extract the band-bending parameter ζ [used in Eq. (1)], i.e., the standard linear VB-edge extrapolation method [29] or the recently published VB DOS fitting method of Swallow *et al.* [28]. The VB DOS fitting approach yields values of V_{bb} that are systematically more negative by ~ 0.5 eV compared to the linear VB-edge extrapolation method, while ΔV_{bb} is, to a reasonable approximation, independent of the method used. A similar ~ 0.5 -eV systematic shift between these methods should also apply to the synchrotron XPS VB spectra in this work, and this was verified by a comparison of the low BE edges of unbroadened and (instrumental and lifetime) broadened VB DOS that were fitted to a selection of our experimental VB spectra (not shown). Consequently, we have added a right-hand V_{bb} axis to Fig. 6 to indicate the approximate values expected using the VB DOS fitting method, while the left-hand V_{bb} axis corresponds to the standard linear VB-edge extrapolation method. In addition, Fig. 7 shows a schematic diagram of the band bending of the conduction band, using both methods, at the as-received ($\bar{2}01$) β -Ga₂O₃ surface before and after each of the surface treatments, and also for the bare ($\bar{2}01$) β -Ga₂O₃ surface prepared by 600 °C heating of the H₂SO₄-treated surface.

A number of conclusions can be drawn from Fig. 6 and Fig. 7 irrespective of the choice of method: (1) β -Ga₂O₃ ($\bar{2}01$) surfaces with high OH coverages, particularly those prepared by wet O₂ annealing, are unlikely to be electron depleted as there is no evidence of any upward band bending using either method, and (2) bare β -Ga₂O₃ ($\bar{2}01$) surfaces are highly

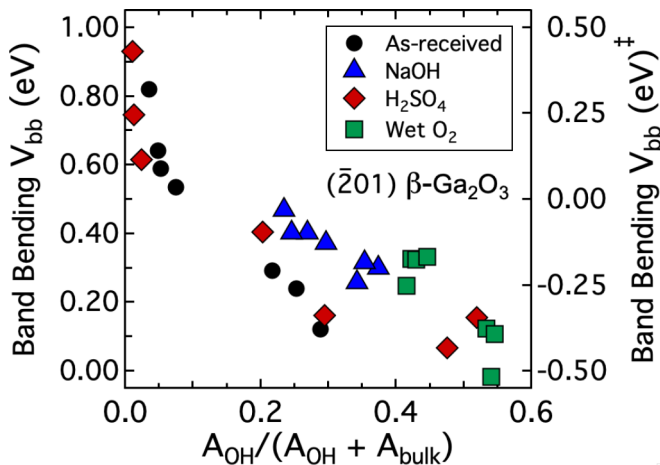


FIG. 6. Band bending V_{bb} versus OH-fraction A_{OH} for the as-received, NaOH-treated, H₂SO₄-treated, and wet O₂ annealed β -Ga₂O₃($\bar{2}01$) samples during the first 600 °C heating cycle. [Note: (1) the left-hand axis shows V_{bb} determined using the standard linear VB-edge extrapolation method [29], while the right-hand axis corresponds to the VB DOS fitting method [28]; (2) In each case, positive values of V_{bb} indicate upward surface band bending and electron depletion, while negative values of V_{bb} correspond to downward band bending and electron accumulation.]

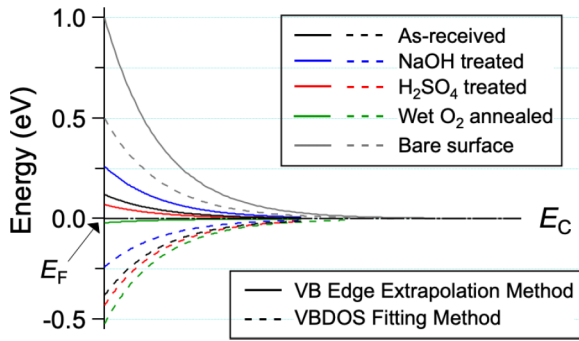


FIG. 7. Schematic diagram of the band bending of the conduction band at the as-received, NaOH-treated, H_2SO_4 -treated, wet O_2 (600°C) annealed, and bare (OH-free) surfaces of $\beta\text{-Ga}_2\text{O}_3$ ($\bar{2}01$) determined using (i) the standard linear VB-edge extrapolation method (solid traces) and (ii) the VB DOS fitting method (dashed traces). Note: (1) the bare surface was prepared by H_2SO_4 treatment followed by 600°C heating; (2) in the absence of surface band-gap narrowing [46] the band bending of the conduction band should match that of the valence band; (3) the position of the Fermi level (E_F) is at 0 eV and is coincident with the conduction-band minimum (E_C) in the bulk of the sample as $E_C - E_F \approx 0$ for the Sn-doped $\beta\text{-Ga}_2\text{O}_3$ single-crystal wafers used in this work.

likely to be electron depleted as large positive V_{bb} values of at least +0.5 eV were obtained using both methods. The main uncertainty concerns the nature of the as-received $\beta\text{-Ga}_2\text{O}_3$ ($\bar{2}01$) surface—this would be weakly depleted (i.e., close to flat bands) using the standard linear VB-edge extrapolation method [29], while the VB DOS fitting method of Swallow *et al.* [28] predicts the presence of downward band bending and electron accumulation. Further experimental measurements such as variable temperature magnetotransport measurements [6] or electrochemical capacitance-voltage measurements [7] would be useful in confirming the presence or absence of any electron accumulation at hydroxyl-terminated $\beta\text{-Ga}_2\text{O}_3$ ($\bar{2}01$) surfaces. Alternatively, evidence can possibly be obtained by observing zero-binding energy XPS emission directly from any surface electron accumulation layer [11] or by measuring the direction of the near-surface band bending using depth-resolved core-level XPS [47,48].

V. CONCLUSIONS

Core-level and valence-band synchrotron XPS were used to investigate the relationship between the OH termination and band bending at ($\bar{2}01$) $\beta\text{-Ga}_2\text{O}_3$ surfaces. Removal of the OH termination produced large upward shifts in band bending of up to 1.0 eV, almost twice that previously reported [22,23,28], due to the use of surface-sensitive synchrotron radiation ($h\nu = 150\text{ eV}$, $\lambda \sim 6.2\text{ \AA}$). Simple surface treatments

and UHV heating were used to modify the band bending of as-received ($\bar{2}01$) $\beta\text{-Ga}_2\text{O}_3$ surfaces by changing the nature and stability of the OH termination. NaOH treatment consistently produced an upward shift in band bending, compared to as-received surfaces, while significantly increasing the thermal stability of the OH coverage. Conversely, H_2SO_4 treatment produced a downward shift in band bending and a significant reduction in the thermal stability of the OH termination, allowing almost complete OH removal via 600°C heating in UHV. Wet O_2 (600°C) annealing produced the most-stable OH coverage, that was resilient to UHV heating at 750°C and also the strongest downward shift in band bending. These effects can be explained by differences in the electron-donating and hydrogen-bonding ability of the $\text{O}_s\text{-H}_w$ and $\text{Ga}_s\text{-O}_w\text{H}_w$ hydroxyl species, that are created by the dissociative adsorption of H_2O on $\beta\text{-Ga}_2\text{O}_3$ surfaces, although differences in the $\text{O}_s\text{-H}_w$ and $\text{Ga}_s\text{-O}_w\text{H}_w$ bond strengths may also play a role. The dissociative rehydroxylation of bare ($\bar{2}01$) $\beta\text{-Ga}_2\text{O}_3$ surfaces in atmosphere was found to be a relatively slow process, which allowed $\beta\text{-Ga}_2\text{O}_3$ surfaces with different levels of electronic band bending to be prepared. The ability to modify the band bending at $\beta\text{-Ga}_2\text{O}_3$ surfaces by chemically manipulating the surface OH termination may prove useful for the fabrication of metal-semiconductor contacts and heterojunctions to this material. For example, the thermally stable downward shift in surface band bending produced by wet O_2 annealing should be advantageous for Ohmic contacts as these rely on the formation of low (or narrow) potential barriers, while the strong upward band bending at bare (OH-free) surfaces should assist the formation of Schottky contacts for which high potential barriers are necessary. Finally, a comparison of two different methods to determine the absolute band bending showed that bare ($\bar{2}01$) $\beta\text{-Ga}_2\text{O}_3$ surfaces are characterized by strong (~ 0.5 to 1.0 eV) upward band bending and an associated near-surface electron depletion layer. This can be completely removed by the hydroxylation of the surface, particularly using wet O_2 (600°C) annealing.

ACKNOWLEDGMENTS

We gratefully acknowledge beamtime and the expert assistance of B. Cowie, L. Thomsen, and A. Tadich at the Australian Synchrotron, Victoria, Australia. M.W.A. is grateful for access to the resources of the Thompson Library at The Ohio State University. This work was financially supported by the MacDiarmid Institute for Advanced Materials and Nanotechnology. We are particularly grateful to Tim Veal (University of Liverpool, UK) for sharing Joel Varley's (Lawrence Livermore National Laboratory, USA) theoretical valence band density of states used in Ref. [28].

- [1] M. Higashiwaki and G. H. Jessen, *Appl. Phys. Lett.* **112**, 060401 (2018).
- [2] S. J. Pearton, F. Ren, M. Tadjer, and J. Kim, *J. Appl. Phys.* **124**, 220901 (2018).
- [3] X. Chen, F. Ren, S. Gu, and J. Ye, *Photonics Res.* **7**, 381 (2019).

- [4] T. Kamimura, K. Sasaki, M. Hoi Wong, D. Krishnamurthy, A. Kuramata, T. Masui, S. Yamakoshi, and M. Higashiwaki, *Appl. Phys. Lett.* **104**, 192104 (2014).
- [5] M. J. Tadjer, N. A. Mahadik, J. A. Freitas, E. R. Glaser, A. D. Koehler, L. E. Luna, B. N. Feigelson, K. D. Hobart, F. J. Kub,

- and A. Kuramata, Gall. Nitride Mater. Devices XIII, Proc. SPIE **10532**, 1053212 (2018).
- [6] M. W. Allen, C. H. Swartz, T. H. Myers, T. D. Veal, C. F. McConville, and S. M. Durbin, *Phys. Rev. B* **81**, 075211 (2010).
- [7] S. K. Vasheghani Farahani, T. D. Veal, J. J. Mudd, D. O. Scanlon, G. W. Watson, O. Bierwagen, M. E. White, J. S. Speck, and C. F. McConville, *Phys. Rev. B* **90**, 155413 (2014).
- [8] L. F. J. Piper, L. Colakerol, P. D. C. King, A. Schleife, J. Zúñiga-Pérez, P. A. Glans, T. Learmonth, A. Federov, T. D. Veal, F. Fuchs, V. Muñoz-Sanjosé, F. Bechstedt, C. F. McConville, and K. E. Smith, *Phys. Rev. B* **78**, 165127 (2008).
- [9] K. H. L. Zhang, R. G. Egdell, F. Offi, S. Iacubucci, L. Petaccia, S. Gorovikov, and P. D. C. King, *Phys. Rev. Lett.* **110**, 056803 (2013).
- [10] V. Jovic, S. Moser, A. Papadogianni, R. J. Koch, A. Rossi, C. Jozwiak, A. Bostwick, E. Rotenberg, J. V. Kennedy, O. Bierwagen, and K. E. Smith, *Small* **16**, 1903321 (2020).
- [11] P. D. C. King and T. D. Veal, *J. Phys.: Condens. Matter* **23**, 334214 (2011).
- [12] P. D. C. King, T. D. Veal, D. J. Payne, A. Bourlange, R. G. Egdell, and C. F. McConville, *Phys. Rev. Lett.* **101**, 116808 (2008).
- [13] R. Heinhold, G. T. Williams, S. P. Cooil, D. A. Evans, and M. W. Allen, *Phys. Rev. B* **88**, 235315 (2013).
- [14] R. Heinhold, S. P. Cooil, D. A. Evans, and M. W. Allen, *J. Phys. Chem. C* **118**, 24575 (2014).
- [15] A. M. Hyland, R. A. Makin, S. M. Durbin, and M. W. Allen, *J. Appl. Phys.* **121**, 024501 (2017).
- [16] G. T. Dang, T. Uchida, T. Kawaharamura, M. Furuta, A. Hyndman, R. Martinez, S. Fujita, R. J. Reeves, and M. W. Allen, *Appl. Phys. Express* **9**, 041101 (2016).
- [17] H. Von Wenckstern, D. Splith, F. Schmidt, M. Grundmann, O. Bierwagen, and J. S. Speck, *APL Mater.* **2**, 046104 (2014).
- [18] J. Michel, D. Splith, J. Rombach, A. Papadogianni, T. Berthold, S. Krischok, M. Grundmann, O. Bierwagen, H. Von Wenckstern, and M. Himmerlich, *ACS Appl. Mater. Interfaces* **11**, 27073 (2019).
- [19] J. Rombach, A. Papadogianni, M. Mischo, V. Cimalla, L. Kirste, O. Ambacher, T. Berthold, S. Krischok, M. Himmerlich, S. Selve, and O. Bierwagen, *Sens. Actuators, B* **236**, 909 (2016).
- [20] A. R. McNeill, A. R. Hyndman, R. J. Reeves, A. J. Downard, and M. W. Allen, *ACS Appl. Mater. Interfaces* **8**, 31392 (2016).
- [21] T. Berthold, S. Katzer, J. Rombach, S. Krischok, O. Bierwagen, and M. Himmerlich, *Phys. Status Solidi* **255**, 1700324 (2018).
- [22] A. Navarro-Quezada, Z. Galazka, S. Alamé, D. Skuridina, P. Vogt, and N. Esser, *Appl. Surf. Sci.* **349**, 368 (2015).
- [23] T. C. Lovejoy, R. Chen, X. Zheng, E. G. Villora, K. Shimamura, H. Yoshikawa, Y. Yamashita, S. Ueda, K. Kobayashi, S. T. Dunham, F. S. Ohuchi, and M. A. Olmstead, *Appl. Phys. Lett.* **100**, 181602 (2012).
- [24] Y. Huan, S. Sun, C. Gu, W. Liu, S. Ding, H. Yu, C. Xia, and D. W. Zhang, *Nanoscale Res. Lett.* **13**, 246 (2018).
- [25] M. H. Lee and R. L. Peterson, *APL Mater.* **7**, 022524 (2019).
- [26] Y. Yao, R. Gangireddy, J. Kim, K. K. Das, R. F. Davis, and L. M. Porter, *J. Vac. Sci. Technol. B* **35**, 03D113 (2017).
- [27] C. Hou, R. M. Gazoni, R. J. Reeves, and M. W. Allen, *Appl. Phys. Lett.* **114**, 033502 (2019).
- [28] J. E. N. Swallow, J. B. Varley, L. A. H. Jones, J. T. Gibbon, L. F. J. Piper, V. R. Dhanak, and T. D. Veal, *APL Mater.* **7**, 022528 (2019).
- [29] S. A. Chambers, T. Droubay, T. C. Kaspar, and M. Gutowski, *J. Vac. Sci. Technol., B: Microelectron. Nanometer Struct.–Process., Meas., Phenom.* **22**, 2205 (2004).
- [30] S. Knight, A. Mock, R. Korlacki, V. Darakchieva, B. Monemar, Y. Kumagai, K. Goto, M. Higashiwaki, and M. Schubert, *Appl. Phys. Lett.* **112**, 012103 (2018).
- [31] J. Furthmüller and F. Bechstedt, *Phys. Rev. B* **93**, 115204 (2016).
- [32] R. Anvari, D. Spagnoli, G. Parish, and B. Nener, *Chem.-Eur. J.* **24**, 7445 (2018).
- [33] A. Kuramata, K. Koshi, S. Watanabe, Y. Yamaoka, T. Masui, and S. Yamakoshi, *Jpn. J. Appl. Phys.* **55**, 1202A2 (2016).
- [34] See Supplemental Material at <http://link.aps.org/supplemental/10.1103/PhysRevB.102.035304> for Tauc plots, atomic force microscope images, and additional synchrotron x-ray photoelectron spectra used to characterize the $(\bar{2}01)$ β -Ga₂O₃ material used in this work.
- [35] S. Tanuma, C. J. J. Powell, Penn D. R., D. R. Penn, and Penn D. R., *Surf. Interface Anal.* **17**, 927 (1991).
- [36] X. Zhou, E. J. M. Hensen, R. A. Van Santen, and C. Li, *Chem.-Eur. J.* **20**, 6915 (2014).
- [37] Y. Ma, X. Zhao, M. Niu, W. Li, X. Wang, C. Zhai, T. Wang, Y. Tang, and X. Dai, *RSC Adv.* **7**, 4124 (2017).
- [38] M. W. Allen, D. Y. Zemlyanov, G. I. N. Waterhouse, J. B. Metson, T. D. Veal, C. F. McConville, and S. M. Durbin, *Appl. Phys. Lett.* **98**, 101906 (2011).
- [39] M. Wagner, P. Lackner, S. Seiler, A. Brunsch, R. Bliem, S. Gerhold, Z. Wang, J. Osiecki, K. Schulte, L. A. Boatner, M. Schmid, B. Meyer, and U. Diebold, *ACS Nano* **11**, 11531 (2017).
- [40] K. Yamaguchi, *Solid State Commun.* **131**, 739 (2004).
- [41] J. Giber, I. V. Perczel, J. Gerblinger, U. Lampe, and M. Fleischer, *Sens. Actuators, B* **18**, 113 (1994).
- [42] F. Réti, M. Fleischer, H. Meixner, and J. Giber, *Sens. Actuators, B* **18**, 138 (1994).
- [43] M. Nagao, K. Yunoki, H. Muraishi, and T. Morimoto, *J. Phys. Chem.* **82**, 1032 (1978).
- [44] T. Morimoto, M. Kiriki, S. Kittaka, T. Kadota, and M. Nagao, *J. Phys. Chem.* **83**, 2768 (1979).
- [45] T. Morimoto and M. Nagao, *J. Phys. Chem.* **78**, 1116 (1974).
- [46] P. D. C. King, T. D. Veal, C. F. McConville, J. Zúñiga-Pérez, V. Muñoz-Sanjosé, M. Hopkinson, E. D. L. Rienks, M. F. Jensen, and P. Hofmann, *Phys. Rev. Lett.* **104**, 256803 (2010).
- [47] T. Nagata, O. Bierwagen, M. E. White, M. Y. Tsai, Y. Yamashita, H. Yoshikawa, N. Ohashi, K. Kobayashi, T. Chikyow, and J. S. Speck, *Appl. Phys. Lett.* **98**, 232107 (2011).
- [48] B. Thielert, C. Janowitz, Z. Galazka, and M. Mulazzi, *Phys. Rev. B* **97**, 235309 (2018).